ARTICLE

Selective conversion of 5-hydroxymethylfurfural to cyclopentanone derivatives over Cu-Al_2O_3 and Co-Al_2O_3 catalysts in water

Received 00th January 20xx,
Accepted 00th January 20xx

DOI: 10.1039/x0xx00000x

www.rsc.org/

Rubén Ramos,[a] Alexios Grigoropoulos,[a] Noémie Perret,[a] Marco Zanella,[a] Alexandros P. Katsoulidis,[a] Troy D. Manning,[a] John B. Claridge[a] and Matthew J. Rosseinsky*[,a]

The production of cyclopentanone derivatives from 5-hydroxymethylfurfural (HMF) using non-noble metal based catalysts is reported for the first time. Five different mixed oxides containing Ni, Cu, Co, Zn and Mg phases on an Al-rich amorphous support were prepared and characterised (XRD, ICP, SEM, TEM, H_2-TPR, NH_3/CO_2-TPD and N_2 sorption). The synthesised materials resulted in well-dispersed high metal loadings in a mesoporous network, exhibiting acid/base properties. The catalytic performance was tested in a batch stirred reactor under H_2 pressure (20 - 50 bar) in the range T = 140 - 180 °C. The Cu-Al_2O_3 and the Co-Al_2O_3 catalysts showed a highly selective production of 3-hydroxymethylcyclopentanone (HCPN, 86 %) and 3-hydroxymethylcyclopentanol (HCPL, 94 %), respectively. A plausible reaction mechanism is proposed, clarifying the role of the reduced metal phases and the acid/basic sites on the main conversion pathways. Both Cu-Al_2O_3 and Co-Al_2O_3 catalysts showed a loss of activity after the first run, which can be reversed by a regeneration treatment. The results establish an efficient catalytic route for the production of the diol HCPL (reported for the first time) and the ketone HCPN from bio-derived HMF over 3d transition metals based catalysts in an environmental friendly medium such as water.

Introduction

Emerging environmental concerns and declining availability of petroleum reserves have promoted worldwide interest in developing alternative technologies to convert sustainable biomass resources into value-added chemicals. Non-edible lignocellulosic biomass can be efficiently transformed via acid-catalysed hydrolysis to C_5 and C_6 monosaccharides,[1,2] which may be further processed (via acid-catalysed dehydration) to produce furanic compounds such as furfural (C_5) and 5-hydroxymethylfurfural (C_6).[3,4] Both furan derivatives are regarded as promising biobased platform molecules, expected to play a critical role in future biorefineries.[5,6,7]

In this context, 5-hydroxymethylfurfural (HMF) can be converted into useful bio-derived products that could serve as building blocks in diverse sectors of the chemical industry, *e.g.*; 2,5-furandicarboxylic acid (FDCA),[8] tetrahydrofuran 2,5-diyldimethanol (THFDM),[9] 2,5-dimethylfuran (DMF),[10] levulinic acid[11] and C_6 linear alcohols[12] (Figure 1). Due to the overfunctionalized nature of HMF, the formation of these compounds involves several chemical transformations (*e.g.* oxidation, hydrogenation, dehydration, hydrogenolysis, ring opening, etc.) which require the presence of multifunctional heterogeneous catalysts.

One particularly challenging reaction is the conversion of HMF into cyclopentanone derivatives in water. These alicyclic compounds are versatile raw materials for the synthesis of products like fragrances, drugs, solvents, pesticides, polymers, etc.[13,14] Therefore, since they are currently mainly produced from petrochemical resources (decarboxylation of adipic acid,[15] oxidation of cyclopentene[16] or cyclization of 1,6-hexanediol[17]) under harsh reaction conditions, the efficient manufacture of these commodity chemicals from biomass-derived compounds would be of great significance. Moreover, since production of HMF from sugars is carried out in water, a renewable, safe and low cost solvent, further processing of HMF in water is especially convenient.[18,19]

Although furfural conversion to cyclopentanone and cyclopentanol has been previously described in aqueous medium (140 - 190 °C; 20 - 80 H_2 bar),[14,20] the analogous transformation for HMF has been scarcely studied. Ohyama *et al*. recently reported the conversion of HMF to 3-hydroxymethylcyclopentanone (HCPN; 86 %) in water and under hydrogen pressure (140 °C; 30 - 80 H_2 bar), using supported Au nanoparticles[13] and Pt/SiO_2 in combination with acid-base metal oxides.[21] By contrast, we reported the formation of HCPN from HMF in water by using a 3d metal Ni-Al catalyst, as opposed to the use of noble metals catalysts.[22]

The conversion of HMF into alicyclic compounds proceeds through initial hydrogenation steps on metal particles, followed by furan ring rearrangement catalysed by Lewis acidic sites. However,

[a] *Department of Chemistry, University of Liverpool, Crown Street, Liverpool L69 7ZD, U.K. E-mail: m.j.rosseinsky@liverpool.ac.uk*

†Electronic Supplementary Information (ESI) available: [Catalysts characterization, additional results, NMR spectra and GC-MS patterns]. See DOI: 10.1039/x0xx00000x

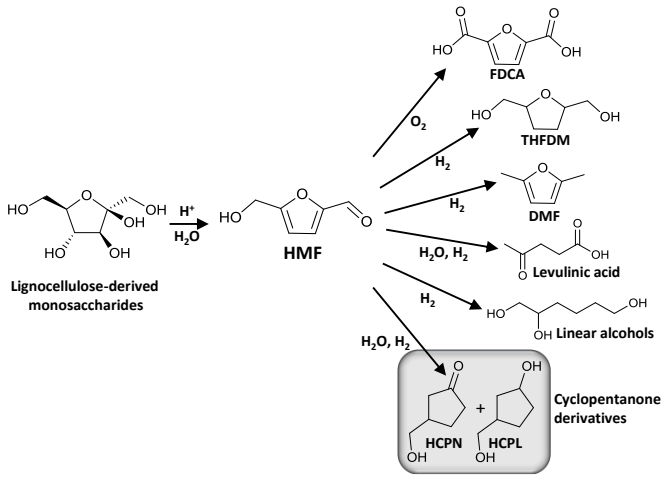

Figure 1. Catalytic transformation of HMF to bio-derived products with potential industrial applications (HCPN and HCPL are the targeted products of the present work).

some fundamental aspects of the reaction mechanism like the role of metal sites on ring-opening/closure steps or the influence of basic sites in condensation reactions remain unclear. Moreover, the formation of the fully hydrogenated 3-hydroxymethylcyclopentanol (HCPL) from HMF has not been reported to date. Thus, the development of novel heterogeneous catalysts based on inexpensive and abundant 3d transition metals, exhibiting water stability and high activity/selectivity towards HCPN and/or HCPL remains a challenging task.

In this regard, the synthesis of mixed oxides derived from layered double hydroxides (LDH) has attracted considerable attention as multifunctional catalyst precursors, due to their ability to accommodate a large variety of redox-active divalent and trivalent cations in a Brønsted base framework. The subsequent calcination and reduction steps afford high metal loadings homogenously dispersed in a mesoporous network, with good thermal stability.[23] Likewise, the synergetic effects between metal and oxide phases may generate acid-base active sites, which are expected to contribute to the efficient rearrangement of HMF intermediates into alicyclic compounds. In this respect, the use of different M^{2+} cations may allow tailoring of the catalytic properties and enhancement of the selectivity toward the targeted products.[24]

In this work, five different mixed oxides containing Ni, Cu, Co, Zn and Mg, on alumina amorphous support were prepared. The synthesised materials were widely characterised and investigated as catalysts for the one-pot conversion of HMF to cyclopentanone derivatives in water. High selectivity towards either HCPN or HCPL was observed depending on the catalyst and the operation conditions applied. The obtained product distribution was correlated with the hydrogenating ability and acid-base properties of the catalysts. The effects of reaction temperature (140 - 180 °C) and H_2 pressure (20 - 50 bar) on the performance of the most promising catalysts were also examined in terms of HCPN and HCPL production. Equally, catalyst stability and reusability were evaluated by catalytic and characterization studies of the used catalysts. This approach may establish a consistent understanding of the design of heterogeneous catalyst for the competitive production of cyclopentanone derivatives from lignocellulose-derived HMF in water.

Experimental

Catalyst preparation

Catalyst precursors were prepared by co-precipitation using the urea-based method developed by Constantino *et al*.[25] Firstly, a calculated mass of urea (Sigma) was weighed into glass vials (27 ml) and combined with distilled water using a Chemspeed Accelerator SLT synthesis platform. Then, a mixture of 1.5 M aqueous solutions of $AlCl_3{\cdot}6H_2O$ (Fluka; ≥ 99%) and the corresponding metal precursors were dispensed into those vials using an Eppendorf epMotion 5075PC pipetting robot. The precursors used as Ni, Cu, Co, Mg, and Zn sources were: $NiCl_2{\cdot}6H_2O$ (Aldrich; ≥ 99.9%), $Cu(NO_3)_2{\cdot}3H_2O$ (Fluka), $CoCl_2{\cdot}6H_2O$ (Fluka), $MgCl_2{\cdot}6H_2O$ (Sigma-Aldrich; ≥ 99%) and $ZnCl_2$ (Aldrich; ≥ 99.99%), respectively. The volumes of the solutions and the mass of urea were selected to set the following molar ratios; $n_{Al}/(n_{Me}+n_{Al}) = 0.45$ and $n_{urea}/(n_{Me}+n_{Al}) = 3.3$. The vials were heated to 95 °C (1.5 °C min^{-1}) and stirred under reflux. After aging for 65 h, the solutions were cooled to room temperature and filtered. In order to remove residual Cl, the precipitated materials were left in suspension with NH_4HCO_3 (Alfa Caesar) for 5 h. Subsequently, the samples were filtered, washed with distilled water and dried at 2 °C min^{-1} to 120 °C for 5 h in static air. Finally, the synthesised materials were calcined under air (75 cm^3 min^{-1}) at 500 °C for 5 h (heating ramp 5 °C min^{-1}) and reduced under H_2 (100 cm^3 min^{-1}) at 500 °C (700 °C in case of Co containing sample) for 5 h (heating ramp 5 °C min^{-1}). The catalysts were then passivated at room temperature for 3 h under a flow of 1% v/v O_2/N_2 (100 cm^3 min^{-1}).

Catalyst characterization

The synthesised catalysts were characterised by X-Ray diffraction on a Panalytical X'Pert Pro diffractometer with Co $K_{\alpha 1}$ radiation (λ = 1.7890 Å). Samples were scanned at 0.023° s^{-1} over the range $10° < 2\theta < 80°$ for phase identification using reference standards. The mean metal crystallite size was calculated using the Scherrer equation. Metal content of the catalysts was measured by inductively coupled plasma optical emission spectroscopy (ICP-OES) after digestion in acid (25 mg of sample in 10 ml HCl 37 %) and dilution with water (1:10 v/v). Textural properties were measured using nitrogen adsorption–desorption isotherms at 77 K with a Micromeritics TRISTAR II instrument. Prior to the measurement, the samples were outgassed at 120 °C under vacuum for 20 h. Specific surface area was calculated using the BET equation in the range $0.05 < P/P_0 < 0.2$, whereas pore volume and pore size distribution were determined by the BJH method.

Temperature programmed reduction (TPR) was measured using a Quantachrome ChemBET 3000 unit; *ca.* 50 mg of sample were loaded into a quartz cell and heated up to 750 °C at 5 °C min^{-1} under a flow of 5% v/v H_2/N_2 (100 cm^3 min^{-1}). The acid and base features of the catalysts were determined in a Micrometrics 2920 equipment by temperature programmed desorption (TPD) of ammonia and carbon dioxide, respectively. Previously, the samples were outgassed under a stream of He (20 cm^3 min^{-1}) heating at 5 °C min^{-1}

up to 550 °C. For NH_3-TPD curves, the samples were cooled to 180 °C and saturated under an ammonia stream (5% v/v NH_3/He; 20 cm^3 min^{-1}) for 30 min. Subsequently, the physically adsorbed ammonia was removed by flowing helium (20 cm^3 min^{-1}) for 30 min. Thereafter, the chemically adsorbed ammonia was desorbed by heating to 550 °C with a rate of 10 °C min^{-1} in flowing He (20 cm^3 min^{-1}). The CO_2-TPD experiment was initiated by cooling the sample to 50 °C followed by saturation with a flow of 5% v/v CO_2/He (20 cm^3 min^{-1}) for 30 min. Afterward, the physisorbed carbon dioxide was removed by flowing He (20 cm^3 min^{-1}) for 30 min. Finally, the chemically adsorbed CO_2 was desorbed by heating the sample to 650 °C (heating rate of 10 °C min^{-1}) in flowing He (20 cm^3 min^{-1}). The variation of ammonia and carbon dioxide concentration in the effluent helium stream was recorded continuously using a thermal conductivity detector (TCD).

IR spectra were collected in ATR mode using a FT-IR Perkin-Elmer Spectrum 100 spectrometer (4 cm^{-1} resolution, 16 scans). Thermogravimetric analysis (TGA) were carried out on a Q600 TA Instruments; *ca*. 10 mg of sample were loaded into an alumina microcrucible and heated to 800 °C at 10 °C min^{-1} in flowing N_2 at 100 cm^3 min^{-1}. Elemental analysis (C and H content) of the used catalysts were carried out on a Thermo EA1112 Flash CHNS Analyser. SEM images were taken using a Hitachi S-4800 Field-Emission Scanning Electron Microscope. Prior to recording the SEM micrographs, the samples were sputter-coated with Au to reduce charging effects. TEM images were obtained with a JEOL 2100 transmission electron microscope. EDX mapping was performed with a windowless EDAX EDX detector using the microscope in STEM mode. Previous to the observation, the samples were dispersed in acetone, stirred in an ultrasonic bath and deposited on a carbon-coated Cu grid.

Catalytic experiments and product analysis

The performance of the catalysts was studied in a high pressure 100 ml batch stirred reactor (Parr Instrument Co.) equipped with a Parr 4848 acquisition interface. A glass liner was loaded with 45 ml of an aqueous solution of HMF (0.04 M) and 0.02 - 0.06 g of catalyst, and placed into the stainless steel reactor. The reactor was then sealed, flushed with N_2 and heated to the required reaction temperature (140 - 180 °C). Once the desired temperature was reached, the vessel was pressurized to 20 - 50 bar of H_2 and the stirring speed was increased to 600 rpm. After the reaction, the product identification and quantification was carried out by GC-MS (Agilent 6890N GC with a 5973 MSD detector) and GC (Agilent 7890A GC with a FID detector), respectively. Both instruments were equipped with a DB-WAXetr capillary column (60 m, 0.25 mm i.d., 0.25 µm). Standard reference compounds like HMF (Sigma; > 99 %), furan-2,5-diyldimethanol (FDM; Manchester Organics), THFDM (Ambinter) and HCPL (Ambinter) were used for identification and calibration measurements. Identification of 1-hydroxyhexane-2,5-dione (HHD), 4-hydroxy-4-hydroxymethyl-2-cyclopentenone (HHCPN) and HCPN was carried out via a combination of GC-MS and NMR spectroscopy using a Bruker AVANCE III HD spectrometer. Details concerning conversion, yield and selectivity calculations are given elsewhere.[22]

Results and discussion

Characterization analysis

The synthesised hydrotalcite precursors are described by the general formula $[M^{2+}_{1-x}Al^{3+}_x(OH)_2][(CO_3^{2-})_{x/2}]\cdot mH_2O$, where M^{2+} are the divalent cations: Ni^{2+}, Cu^{2+}, Co^{2+}, Zn^{2+}, and Mg^{2+}. The structure of these layered double hydroxides corresponds to brucite-like sheets, replacing a fraction of M^{2+} by Al^{3+} and conferring a positive layer charge. This charge is balanced by interlayer CO_3^{2-} anions, whereas intercalated H_2O molecules provide hydrogen bonding between adjacent brucite layers. Five different layered double hydroxides (labelled M-Al-P) were prepared with the same M^{2+}/Al^{3+} ratio (x_{Al} = 0.45), as described in the experimental section.

The XRD patterns (2θ = 10 - 80 °) of the precursors prepared with Ni, Co, Zn and Mg show the characteristic peaks of hydrotalcite-like materials (Figure 2a).[26] Well-defined diffraction peaks of the three basal (003), (006) and (009) planes, and the reflections associated with the non-basal (110) and (113) planes can be identified. The latter peaks reveal good dispersion of the metal cations in the hydroxide layers.[27] These results are in agreement with the work of Constantino *et al.*,[25] reporting a well-crystallized layered structure

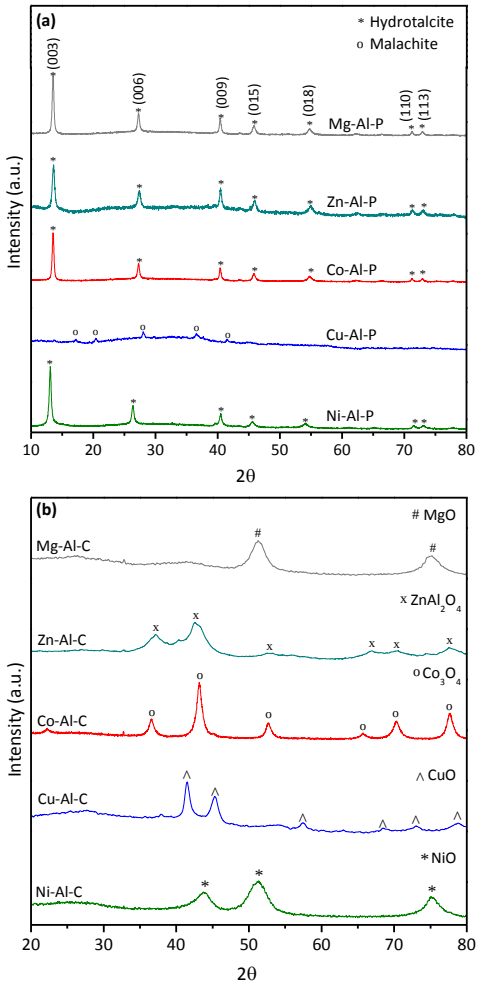

Figure 2. (a) XRD patterns of the as-synthesised precursor materials and (b) XRD patterns of the calcined materials (air, 500 °C, 5 h).

with the employed synthesis parameters (pH ≈ 8.5; 65 h; 95 °C). However, one exception should be noted in the case of the Cu-Al-P diffraction pattern, in which an essentially amorphous material is observed with traces of malachite phase ($Cu_2(OH)_2(CO_3)$). Several authors have claimed the difficulty in obtaining pure Cu-Al hydrotalcite type compounds due to the Jahn-Teller effect of Cu^{2+} ions (d^9 electron configuration) which destabilises octahedral geometry and favours other phases like malachite.[28,29,30]

The as-synthesised precursor materials were calcined at 500 °C for 5 hours in air (heating rate 5 °C min^{-1}) to obtain the corresponding mixed oxides. During calcination, H_2O molecules and carbonate anions are initially removed, followed by dehydroxylation of the surface and partial oxidation of M^{2+} at higher temperatures. Under these conditions, the double-layered structure collapses and the metal ions coordinate with adjacent oxygen atoms and work as pillars forming an open mesoporous structure. As a result, calcination leads to metal-like oxides with an Al-rich amorphous component (labelled M-Al-C). Figure 2b shows the XRD patterns of the calcined materials. The samples prepared with Ni or Cu show peaks characteristic of cubic NiO (JCPDS 70-0989) and monoclinic CuO (65-2909), respectively. For Co-Al-C and Zn-Al-C the initial layered structures were converted to a spinel-like phase of composition Co_3O_4 (80-1535) and $ZnAl_2O_4$ (73-1961). It should be noted that for Co-Al-C, the observed diffraction peaks may be also ascribed to $CoAl_2O_4$, since it is not possible to distinguish between these two phases by PXRD.[31] For Mg-Al-C, the calcination treatment resulted in the formation of MgO periclase (03-0998).

The reducibility of the calcined samples was determined by hydrogen temperature-programmed reduction (Figure 3a). The H_2-TPR profiles of Zn-Al-C and Mg-Al-C do not show any peak attributed to H_2 consumption, suggesting that the oxide phases formed in these samples are not reduced under the analysis conditions (5% v/v H_2/N_2; 20 - 750 °C). For Ni-Al-C, the TPR curve exhibits a single broad peak centered on 577 °C, which has been previously ascribed to the reduction of Ni^{2+} to Ni^0. In this respect, it is well known that the introduction of Al^{3+} into the NiO lattice enhances its stability and increases the reduction temperature.[32] The reduction profile of Cu-Al-C presents two overlapping peaks at 288 and 356 °C, assigned to the reduction of highly and poorly dispersed Cu oxide species on alumina, respectively.[33,34] The reduction profile of Co-Al-C shows two H_2 consumption peaks in two different temperature intervals. The low-temperature peak (435 °C) is attributed to partial reduction of Co_3O_4 to CoO, whereas the high-temperature peak (625 °C) is typically assigned to the reduction of CoO to metallic cobalt.[35,36] However, it should be noted that both the temperature interval and the area of the H_2-TPR peaks can be also influenced by the interaction with the alumina support and the metal crystallite sizes.[37]

The calcined samples were reduced under a stream of H_2 (100 cm^3 min^{-1}; 5 h) at a temperature determined by the respective H_2-TPR profile and then passivated (1% v/v O_2/N_2; 100 cm^3 min^{-1}; 20 °C for 3 h). Figure 3b shows the XRD patterns of the final catalysts after the reduction treatment (M-Al_2O_3). The samples containing Ni, Cu and Co show peaks corresponding to cubic Ni (70-0989), Cu (03-1005) and Co (01-1259) metallic phases. The disappearance of cobalt spinel-like phase after the reduction step indicates the prevalence of Co_3O_4 over $CoAl_2O_4$ in the calcined precursor Co-Al-C,

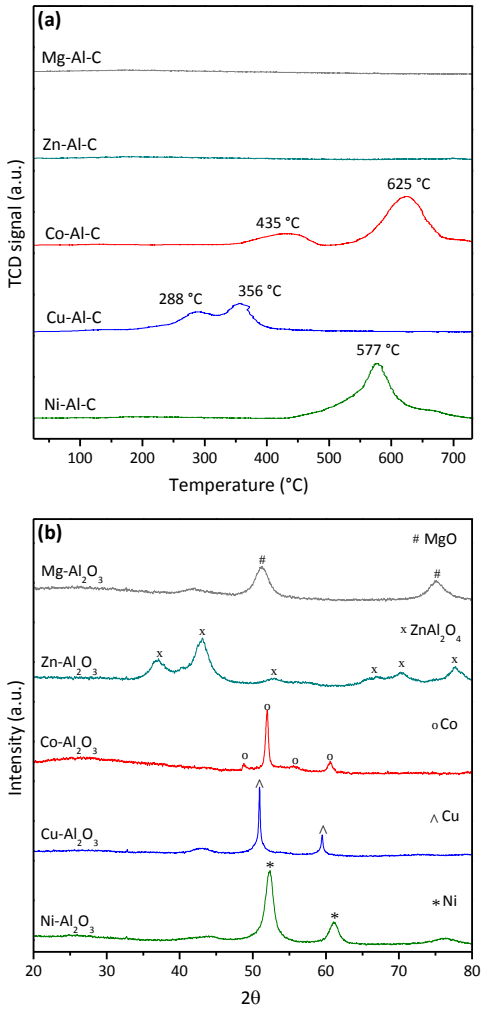

Figure 3. (a) H_2-TPR curves (5 % v/v H_2/N_2) of the calcined precursors and (b) XRD patterns of the reduced catalysts (H_2, 500/700 °C, 5 h). Only Ni, Cu and Co are reduced to the respective metallic phase under these conditions.

since only Co_3O_4 can be reduced below 800 °C.[38] By contrast, Zn-Al_2O_3 and Mg-Al_2O_3 catalysts show identical XRD pattern to the calcined samples. This corroborates the H_2-TPR results and confirms that the reduction treatment does not affect these materials, as expected from their redox chemistry.

The composition of the prepared catalysts was determined by ICP and TGA analysis (Table 1). The Al molar fraction for the samples containing Ni, Co and Zn lies in the range x_{Al} = 0.42 - 0.52, similar to the one introduced in the synthesis of the hydrotalcite precursors (x_{Al} = 0.45). On the other hand, the Al molar fraction of the Mg-Al_2O_3 sample is higher (x_{Al} = 0.60), which could be related to the higher solubility of $Mg(OH)_2$ than aluminium hydroxide in the synthesis solution (pH ≈ 8.5).[25] A higher final Al molar ratio is also found in Cu-Al_2O_3 (x_{Al} = 0.76) which is not unexpected since a different precursor material was used (*vide supra*) and is indicative of incomplete precipitation of Cu during the synthesis of that precursor.

The prepared catalysts exhibit type IV N_2 adsorption-desorption isotherms with significant adsorption of N_2 at intermediate relative pressure ($0.2 < P/P_0 < 0.8$) due to the filling of the mesopores and

Table 1. Physicochemical properties of the synthesised catalysts.

Catalyst	Composition[a]	M[b] (wt%)	d_M[c] (nm)	Textural properties[d]			Acid properties[e]		Base properties[f]	
				S_{BET} (m^2/g)	V_p (cm^3/g)	D_p (nm)	T[g] (°C)	µmol NH_3/g	Strength	µmol CO_2/g
$Ni-Al_2O_3$	$Ni_{0.58}Al_{0.42}O_{1.40}$	50/46	9	98	0.236	10	276	252	Low	31
									Medium	41
									High	115
$Cu-Al_2O_3$	$Cu_{0.24}Al_{0.76}O_{1.24}$	26/24	52	75	0.180	10	269	99	Low	130
									Medium	116
									High	-
$Co-Al_2O_3$	$Co_{0.56}Al_{0.44}O_{1.48}$	44/45	28	96	0.198	9	276	236	Low	32
									Medium	35
									High	196
$Zn-Al_2O_3$	$Zn_{0.48}Al_{0.52}O_{1.59}$	29	5	95	0.170	7	260	109	Low	45
									Medium	60
									High	93
$Mg-Al_2O_3$	$Mg_{0.40}Al_{0.60}O_{1.26}$	20	6	77	0.127	6	266	113	Low	25
									Medium	26
									High	46

[a] Based on ICP and TGA analysis. [b] Metal content calculated from ICP/SEM-EDX measurements. [c] Mean metal crystallite size based on XRD (Scherrer equation). [d] BET surface area (S_{BET}), pore volume (V_p) and pore diameter (D_p) calculated from N_2 adsorption isotherms at 77 K. [e] Acid properties from ammonia TPD measurements. [f] Base properties from carbon dioxide TPD measurements. [g] Maximum desorption temperature.

an increase in N_2 uptake at P/P_0 > 0.8 due to voids of the interparticulate space (Figure SI1). The calculated textural properties (Table 1) show that the incorporation of different M^{2+} cations does not significantly change the specific surface area (S_{BET} = 75 - 98 m^2 g^{-1}) and pore volume (V_p = 0.127 - 0.236 cm^3 g^{-1}) of the samples. The calculated pore distributions, according to the BJH method, show average pore-diameter values in the mesoporous range (D_p = 6 - 10 nm), large enough to host the reactant and the intermediate molecules (HMF long axis ≈ 0.9 nm).[39]

Figure 4 shows the NH_3 (4a) and CO_2 (4b) temperature programmed desorption (TPD) of the synthesised catalysts after calcination and reduction treatments. The overall measured amount and strength of acid/basic sites are summarized in Table 1. The NH_3-TPD curves (Figure 4a) show a noticeably higher acid character for $Ni-Al_2O_3$ and $Co-Al_2O_3$ catalysts (252 and 236 µmol NH_3 g^{-1}, respectively). On the other hand, the $Cu-Al_2O_3$ sample adsorbs the lowest amount of ammonia (99 µmol NH_3 g^{-1}), which implies a lower number of active acid sites present. Regarding the acid strength, no significant differences were observed in the ammonia TPD curves, with the maximum NH_3 desorption temperature occurring within a narrow interval 260 - 276 °C.

The total amount of each type of basic sites was determined by integration of the deconvoluted peaks from the TPD curves (Table 1). The CO_2 TPD profiles of $Ni-Al_2O_3$, $Co-Al_2O_3$, $Zn-Al_2O_3$ and $Mg-Al_2O_3$ (Figure 4b) are in accordance with the well-known basic character of hydrotalcite-derived material, showing three different peaks in the interval 95 - 400 °C associated with the adsorption of bicarbonate anions (low-strength), bidentate carbonates (medium-strength) and monodentate species (high-strength).[40,41] For hydrotalcite derived materials, the highest desorption contribution corresponds to monodentate species (46 - 196 µmol CO_2 g^{-1}), indicating the prevalence of high-strength basic sites on these materials. On the contrary, the CO_2-TPD profile of the $Cu-Al_2O_3$ catalyst reveals a considerably larger amount of weak and medium basic sites (130 and 116 µmol CO_2 g^{-1}, respectively) and most importantly the complete absence of strong basic sites.

Representative TEM images of the prepared catalysts are presented in Figure SI2, suggesting that a good metal dispersion degree and homogeneity was achieved for all samples. The observed particle sizes are consistent with those calculated from XRD patterns (d_M, Table 1). Thus, the $Cu-Al_2O_3$ and $Co-Al_2O_3$ materials clearly present a higher average particle diameter (52 and 28 nm, respectively) than the $Ni-Al_2O_3$ catalyst (9 nm). Likewise, Figure SI2d reveals that the $Zn-Al_2O_3$ catalyst is mainly composed of nanoparticles (5 nm) with spherical shape, similar to the morphology reported for $ZnAl_2O_4$ phase.[42]

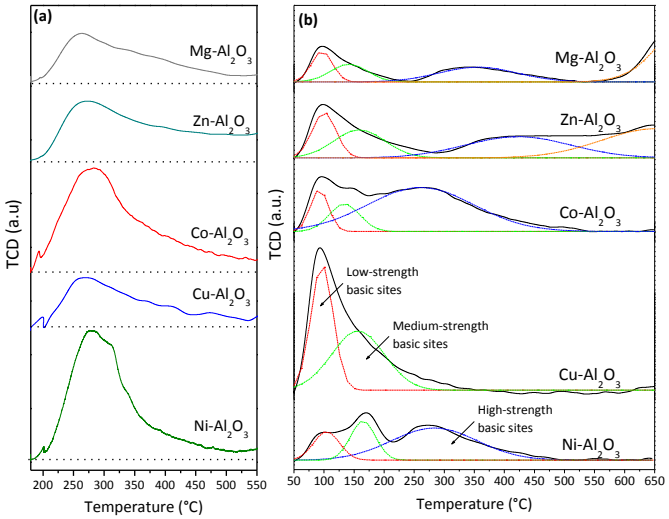

Figure 4. (a) NH_3 (b) and CO_2 temperature programmed desorption (TPD) curves of the prepared catalysts after calcination (air, 500 °C, 5 h) and reduction (H_2, 500/700 °C, 5 h) steps. Dash lines represent the deconvoluted peaks associated with different basic strengths.

5-Hydroxymethylfurfural conversion over mixed oxide catalysts in water

The reaction conditions were selected on the basis of our previous findings regarding the hydrogenation of HMF with various Ni-Al_2O_3 catalysts.[22] We have already shown that formation of HCPN does not take place below 140 °C, but instead the hydrogenation of both the aldehyde group and the furan ring of HMF is favoured (THFDM yield = 100 % at 80 °C). Therefore, batch experiments at 140 °C and 20 bar of hydrogen were performed in order to evaluate the activity of the synthesised catalysts and determine the preferred reaction pathways for the production of cyclopentanone derivatives. During the course of the reaction, hydrogen was continuously supplied to maintain the pressure constant at 20 bar, guaranteeing H_2 excess in the course of the reaction. The effects related to the solubility of the reactant and the intermediates in the aqueous phase were minimized by using a low concentration HMF solution (0.04 M). Mass transfer limitations and internal diffusion resistance were avoided by ensuring small catalytic particle size (< 100 µm) and high stirring speed (600 rpm).[22] Likewise, the amount of catalyst (0.06 g) and overall reaction time (360 min) were also adjusted to detect significant changes in the obtained product distributions. The choice of water as solvent is indispensable to promote furan ring rearrangement into cyclopentanone derivatives, a transformation which does not take place when other solvents are used instead of H_2O such as CH_2Cl_2, MeOH, 1,4-dioxane, n-BuOH or THF.[14,20b]

Table 2 summarizes the product distributions obtained from the conversion of HMF over the synthesised catalysts. The calculated carbon mass balance was higher than 94 % in all experiments, confirming the absence of any significant undetected fraction of by-products. Complete conversion of HMF is achieved with the Ni-Al_2O_3, Cu-Al_2O_3 and Co-Al_2O_3 catalysts. The presence of reduced metal phases on these materials (Figure 3b) ensures the initial hydrogenation of the HMF aldehyde group towards the respective alcohol (FDM), which is the key intermediate for the subsequent formation of cyclopentanone derivatives. On the contrary, the absence of such reduced metal phases on the catalysts containing Zn and Mg (Figure 3b) renders them practically inactive in hydrogenation of HMF (maximum conversion < 11%, Table 2). Commercially available *γ*-Al_2O_3 (Sigma Aldrich) is also catalytically inactive after 6 h (HMF conversion = 1 %).

Within the group of catalytically active materials (*i.e*. Ni-Al_2O_3, Cu-Al_2O_3 and Co-Al_2O_3) significant differences are observed in the final product distribution under identical conditions. The highest yield for HCPN is observed for the Cu-Al_2O_3 catalyst (79 %), followed by the Ni-Al_2O_3 (59 %). Although both catalysts show similar low yields for FDM (4 *vs.* 5 %), the employment of the Ni-Al_2O_3 catalyst results in a significant amount of THFDM (19 %), via the complete hydrogenation of the furan ring. By contrast, this step is totally impeded in the case of the Cu-Al_2O_3 catalyst. Moreover, two more compounds are detected at relatively lower yields, namely HHD (7 %) and HHCPN (5 %).

A similar response has been reported using furfural as a substrate.[43,44] Cu-based catalysts favour hydrogenation of the C=O bond whilst leaving the furan ring intact, leading to furfuryl alcohol as the main product. On the other hand, Ni-based catalysts are capable of hydrogenating the C=C bonds of the furan ring, leading to tetrahydrofuran compounds. Higher selectivity for the hydrogenation of the furan ring could be also attributed to the lower size of Ni particles (d ≈ 9 nm) compared to Cu-Al_2O_3 (d ≈ 52 nm) and Co-Al_2O_3 (d ≈ 28 nm), since hydrogenation of unsaturated rings tends to decrease as particle size increases due to lower substrate adsorption.[45,46]

The high yield of HCPN achieved with the Cu-Al_2O_3 catalyst is accompanied by the absence of any additional hydrogenation of the C=O group that would lead to HCPL. By contrast, when Co-Al_2O_3 is used, HCPN yield decreases to 5 %, whereas HCPL increases to 61 %. Notably, the key intermediate FDM is consumed at a slower rate over the Co-Al_2O_3 catalyst (29 %).

In addition to the compounds listed in Table 2, traces of other by-products derived from C-O hydrogenolysis (3-methylcyclopentanol and 5-methyl-2-furylmethanol) or C-C bond cleavage (cyclopentanone and furfuryl alcohol) were also identified in the product mixture at negligible yields (< 1%). These results confirm that higher temperatures and stronger acidity (typically Brønsted acid sites) are usually required to promote C-O hydrogenolysis and C-C cleavage, due to the higher activation energy of these steps.[44]

Figure 5 depicts the yield of the main products as a function of the reaction time for the active catalysts (Ni-Al_2O_3, Cu-Al_2O_3 and Co-Al_2O_3). All the kinetic curves show a progressive consumption of

Table 2. Product distributions from the conversion of HMF over the synthesised catalysts.[(a)]

		Selectivity (%)					
	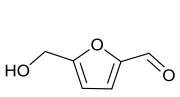	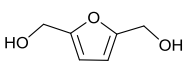	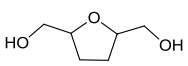	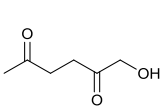	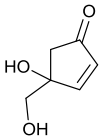	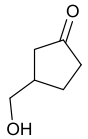	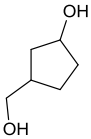
Catalyst	HMF conversion (%)	FDM	THFDM	HHD	HHCPN	HCPN	HCPL
γ-Al_2O_3	1	100	-	-	-	-	-
Ni-Al_2O_3	100	4	19	0	0	59	15
Cu-Al_2O_3	100	5	-	7	5	79	1
Co-Al_2O_3	100	29	1	0	0	5	61
Zn-Al_2O_3	4	86	-	-	-	-	-
Mg-Al_2O_3	11	95	-	-	-	-	-

[(a)] Reaction conditions: 0.23 g_{HMF}, 45 ml H_2O, 0.06 g_{cat}, 140 °C, 20 bar H_2, 600 rpm, 6 h. Carbon mass balance > 94 %.

HMF (concentration close to zero at the end of the experiment) directly related to the selective hydrogenation of the aldehyde group forming FDM as the first intermediate. In all cases, the yield of FDM reaches a maximum at short reaction times (60-120 min), followed by a continuous decrease as it is converted to products. The rate of hydrogenation of HMF to FDM is significantly faster in the case of the Co-Al_2O_3 catalyst, reaching almost complete HMF conversion after 1 h (98 %). On the contrary, the subsequent conversion of FDM is significantly slower compared to Ni-Al_2O_3 and Cu-Al_2O_3 (Figure 5c).

For all three catalysts tested, the ensuing consumption of FDM is accompanied by the formation of HCPN, detected only after FDM yield reaches a maximum (Figure 5). As previously discussed, HCPN is the final major product for Cu-Al_2O_3 (79 %), whereas for Co-Al_2O_3 HCPN is further reduced to HCPL (61 %) via hydrogenation of the ketone C=O group. Importantly, the yield of HCPL shows a pronounced increase once HMF is completely consumed, indicative of the competitive hydrogenation between the aldehyde C=O group of HMF and the ketone C=O group of HCPN (figure 5c). On the other hand, Ni-Al_2O_3 results in the formation of both cyclopentanone derivatives (HCPN; 59 % and HCPL; 15 %), along with THFDM (19 %). The continuous increase of THFDM indicates a higher stability of this compound, as a result of the difficulty in opening saturated furan rings.[44] By contrast, THFDM is practically not observed at any stage of the reaction when Cu-Al_2O_3 or Co-Al_2O_3 are used as catalysts.

Finally, it should be underlined that HHCPN and HHD are detected during the course of the reaction for all catalysts tested. However, their concentration is decreasing once HCPN is formed confirming their intermediate nature. Moreover, the yield of these compounds reaches significant values only for Cu-Al_2O_3, indicating that ring rearrangement and ring closure steps take place at a lower rate. These findings suggest that two independent reaction pathways occur in parallel depending on the type of the catalyst employed. Contrary to the high selectivity towards THFDM observed with Ni-Al_2O_3 at 80 °C,[22] when the temperature is raised to 140 °C rearrangement or opening of the furan ring of FDM is favoured resulting in the targeted cyclopentanone derivatives.

Reaction scheme for the formation pathway of cyclopentanone derivatives from HMF

Based on the analysis of the kinetic curves, a reaction scheme is proposed to describe the major routes involved in the conversion of HMF to HCPN and HCPL. Firstly, the hydrogenation of the aldehyde C=O bond takes place yielding FDM. This hydrogenation step is catalysed by metal species, and compared to furan ring hydrogenation is favoured by the absence of steric hindrance.[46] The subsequent conversion of FDM may proceed through: (i) hydrogenation of the furan ring, (ii) ring rearrangement or (iii) ring-opening (Figure 6). Complete hydrogenation of the furan ring yields THFDM, which is the end product of this pathway. This was separately verified in a control experiment using THFDM as the substrate (Table SI1; entry 1). No conversion of THFDM was observed after 6 h over Ni-Al_2O_3, conclusively demonstrating that the formation of HCPN and HCPL proceeds via ring rearrangement or ring opening of the key intermediate FDM.

The formation of HHCPN by ring rearrangement requires the presence of water and acid sites (pathway ii, figure 6). The need of the latter was proved by performing additional control experiments using FDM as reactant (Table SI1; entries 2 - 4). HHCPN is not formed in the absence of catalytically active sites (blank experiment). By contrast, the experiments performed with γ-Al_2O_3 and Ni-Al_2O_3 (N_2 atmosphere) produced HHCPN (selectivity 66 % and 17 %, respectively), indicating that the presence of acid sites promotes this step. On the other hand, when non-acidic commercially available Ru/C catalyst was employed (Table SI1; entry 5), HHCPN or HCPN were not detected and the sole product identified was the fully hydrogenated THFDM (98 %). These results are contrary to the reported furfural ring rearrangement, which occurs spontaneously in hot water, without the need for catalyst or hydrogen.[20b,20c] The subsequent transformation of HHCPN into HCPN is catalysed by the combination of acid and metal sites, via rapid deoxygenation (dehydration and/or C-O hydrogenolysis) and hydrogenation steps (no intermediates were detected).

The production of HHD from HMF in the presence of water has been previously described to proceed through the acid-catalysed rehydration of FDM followed by ring opening and hydrogenation of the formed intermediates.[47,48] Moreover, HHD may subsequently undergo base-catalysed intramolecular aldol condensation followed

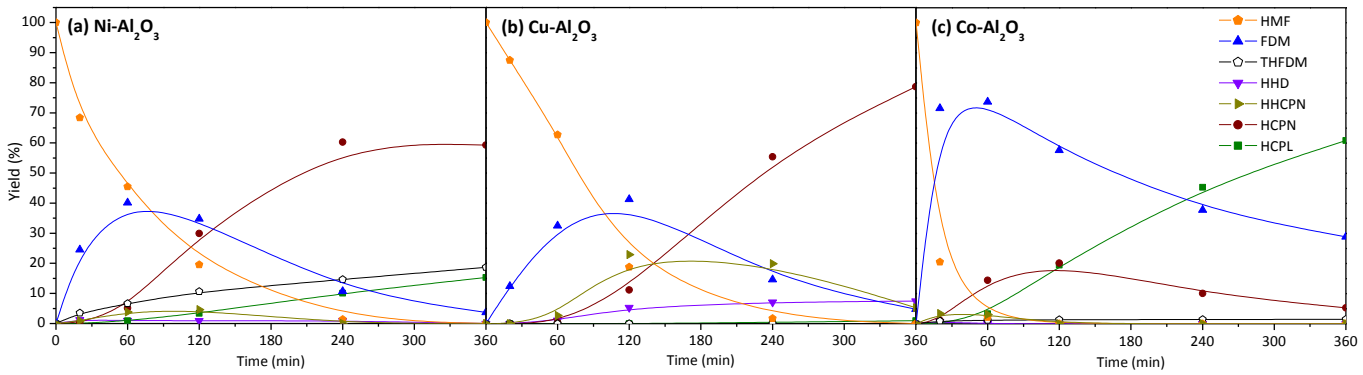

Figure 5. Time evolution of HMF conversion and yield of products over the (a) Ni-Al_2O_3, (b) Cu-Al_2O_3 and (c) Co-Al_2O_3 catalysts (T = 140 °C; P_{H2} = 20 bar).

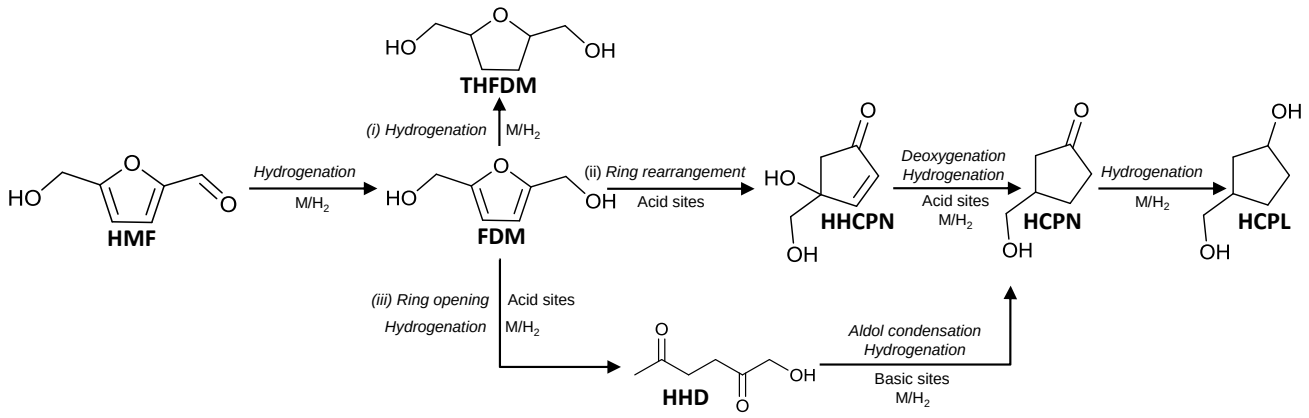

Figure 6. Proposed reaction scheme for the conversion of HMF into HCPN and HCPL.

by hydrogenation, producing HCPN.[13] In order to validate this step, an additional control experiment was carried out over the Co-Al_2O_3 catalyst starting from a solution containing HHD/HCPN (35/59 mol %) (Table SI1; entry 6). After 6 h, complete conversion of HHD into HCPN (3%) and mainly HCPL (82%) was observed, proving that HHD is converted to final products via most likely an aldol condensation reaction (pathway iii, figure 6). In this sense, the higher yield of HHD observed for the Cu-Al_2O_3 catalyst (Table 2), can be correlated with the absence of high-strength basic sites in this material (Figure 4b), which are known to promote aldol condensation reactions.[41]

The final production of HCPL rather than HCPN is strongly influenced by the hydrogenation ability of the catalyst. Therefore, the highest selectivity for HCPL shown by the Co-Al_2O_3 catalysts is associated with the superior interaction of Co particles with the C=O ketone bond.[20c] Overall, this mechanistic study suggests that both ring rearrangement and ring opening of FDM run in parallel and their relative rate strongly depends on the acid/base properties of the catalyst (figure 6, ii and iii).

Influence of temperature and H_2 pressure on HCPN production

The variation of the yield of HCPN at higher temperatures and H_2 pressures was tested using the Cu-Al_2O_3 catalyst. Hydrogen pressure was varied between 20 and 50 bar ([H_2] ≈ 0.421 - 0.942 $cm^3\ g^{-1}$).[49] A maximum temperature of 180 °C was selected in order to keep the reactants and products in the liquid phase and avoid undesirable C-C bond cleavage and coke formation, making the whole process less energy-efficient. Table 3 summarizes the obtained product distributions from HMF conversion over the Cu-Al_2O_3 catalyst after 6 h of reaction at different temperatures and H_2 pressures.

HMF is fully converted to products and, importantly, THFDM is not detected in any run. This fact confirms the selective attraction of the Cu reduced metal phase to the carbonyl group and the strong repulsion towards the furan ring which is not hydrogenated even at higher H_2 pressures.[50] Consequently, a high selectivity towards HCPN is observed, varying between 67 % and 86 %. HHD is only observed in the final products mixture when the reaction is run at low pressure (20 bar), suggesting a faster consumption of this compound as hydrogen pressure increases. This can be related to the hydrogenation step required for the conversion of HHD to HCPN. Equally, as the temperature and the pressure are increased, the yields of FDM and HHCPN decrease due to an enhanced conversion rate. Thus, for T > 160 °C and P_{H2} > 35 bar a highly selective conversion of HMF into HCPN and HCPL is observed.

According to Table 3, the highest yield of HCPN (86 %) is obtained at 180 °C and 20 bar H_2. Nevertheless, excessive intensification of pressure and temperature leads to a decrease of HCPN production due to the hydrogenation of the C=O ketone bond towards HCPL. For example, the reaction carried out at 180 °C and 50 bar H_2 presents the lowest yield of HCPN (67 %) together with the highest production of HCPL (29 %). These results reveal that, unlike the hydrogenation of the furan ring, the hydrogenation of the C=O ketone bond is not totally impeded over the Cu-Al_2O_3 catalysts and its rate can be tailored by varying the reaction conditions.

Influence of temperature and H_2 pressure on HCPL production

Concerning the production of HCPL, a similar study was performed (T = 140 - 180 °C and P_{H2} = 20 - 50 bar) using the Co-Al_2O_3 catalyst, which showed the highest selectivity to HCPL at 140 °C and P_{H2} = 20 bar (61 %, Table 2). Table 4 lists the yields of the main products obtained from the conversion of HMF over the Co-Al_2O_3 catalyst under different reaction conditions.

Table 3. Yield of products from the conversion of HMF over the Cu-Al_2O_3 catalyst. HMF conversion = 100 %.[(a)]

Entry	T (°C)	P (bar)	Yield (%)				
			FDM	HHCPN	HHD	HCPN	HCPL
1	140		5	5	7	79	1
2	160	20	1	6	5	82	3
3	180		0	0	4	86	6
4	140		4	2	0	81	11
5	160	35	0	0	0	85	13
6	180		0	0	0	76	22
7	140		5	0	0	76	16
8	160	50	0	0	0	71	24
9	180		0	0	0	67	29

[(a)] 0.23 g_{HMF}, 45 ml H_2O, 0.06 g_{cat}, 600 rpm, 6 h. Carbon mass balance > 95 %.

When the temperature or the H_2 pressure is raised above standard conditions (T > 140 °C and P_{H2} > 20 bar), the carbon mass balance drops below 95%, suggesting that a non-negligible fraction of products is not detected, in addition to the compounds already described (Figure 6). Most likely, oligomerization of reactive intermediates like FDM and HHCPN is also taking place, forming heavier organic molecules which are hard to detect by the employed GC methods. Oligomerisation reactions are usually promoted by the presence of acid sites at higher temperatures.[7] In this respect, the higher acidity showed by the Co-Al_2O_3 catalyst (Figure 4a) lies in agreement with the augmented production of these heavier by-products.

Nevertheless, a high yield of HCPL is still obtained when the temperature is increased due to complete consumption of FDM. Thus, the yield of HCPL varies within a narrow range of 84 - 89 % for T > 160 °C after 6 h reaction. If the reaction is carried out at T = 140 °C, the formation of HCPL is slightly lower (61 - 77 %), since FDM is not completely converted. Increasing the hydrogen pressure also has a significant impact, reducing the yield of FDM from 29 % to 3 % as the pressure increases from 20 to 50 bar. This fact corroborates the existence of hydrogenation steps during the conversion of FDM into HCPN and HCPL.

In order to improve the production of HCPL by avoiding the formation of undesirable oligomers, two additional experiments were carried out. The amount of catalyst added in the reaction medium was decreased from 0.06 g to 0.02 g and the reaction time was extended to 48 h (entries 10 and 11). The high carbon mass balance obtained in both experiments (> 97 %) suggests that the formation of oligomers practically does not occur. This fact is likely associated to the lower concentration of acid sites in the reaction medium (0.02 *vs*. 0.06 g of catalyst), thus decreasing the extent of acid-catalysed oligomerization steps.[7] The highest yield of HCPL in this work was obtained at 140 °C (reached 94 %, 48 h). However, when the reaction was carried out at 180 °C, HCPL yield significantly decreased (60 %, 48h). According to the kinetic curves presented in Figure SI4, the hydrogenation of HCPN to HCPL is totally impeded after 24 h and the Co-Al_2O_3 catalyst is deactivated. To this end, a detailed investigation concerning the deactivation process of the Cu-Al_2O_3 and the Co-Al_2O_3 catalysts was undertaken.

Table 4. Yield of products from the conversion of HMF over the Co-Al_2O_3 catalyst. HMF conversion = 100 %.[(a)]

Entry	T (°C)	P (bar)	Yield (%)				Carbon mass balance (%)
			FDM	THFDM	HCPN	HCPL	
1	140	20	29	1	5	61	96
2	160		0	1	3	85	89
3	180		0	1	5	84	91
4	140	35	13	1	10	76	97
5	160		0	1	1	88	90
6	180		0	1	4	89	93
7	140	50	3	2	4	77	85
8	160		0	1	1	87	89
9	180		0	1	2	88	90
10[(b)]	140	20	0	0	5	94	99
11[(b)]	180		0	0	38	60	97

[(a)] 0.23 g_{HMF}, 45 ml H_2O, 0.06 g_{cat}, 600 rpm, 6 h.
[(b)] 0.23 g_{HMF}, 45 ml H_2O, 0.02 g_{cat}, 600 rpm, 48 h.

Characterization of used catalysts and reusability studies

The concentration of Cu and Co in the supernatant at the end of the reaction (140 °C; 20 bar H_2) was found less than 0.06 ppm (<0.01 wt % of metal content) according to ICP analysis. Moreover, in a typical hot filtration test, the Cu-Al_2O_3 and Co-Al_2O_3 catalysts were filtered off after 20 min (HMF conversion = 26 % and 66 %, respectively), and the supernatant was left to react under the same conditions for additional 6 h. The analysis of the product mixture after removing the catalyst did not show any additional HMF conversion. Both results prove the absence of any metal leaching into the liquid phase and confirm the heterogeneous nature of the catalytic system.

Samples of the used Cu-Al_2O_3 and Co-Al_2O_3 catalysts were recovered after reaction (T = 140 °C; P = 20 bar H_2) by filtration and dried at room temperature. The TG/DTG curves of the spent Cu-Al_2O_3 sample (Figure SI5a) show a total loss of approximately 28 %. In addition, the elemental microanalysis of the spent catalysts (Figure SI5a inset) reveals a low content of C (2.23 % w/w) together with a relative high content of H (1.98 % w/w). Therefore, the TGA measured weight loss cannot be solely attributed to organic compounds deposited on the surface of the catalyst during the reaction. The XRD pattern of the spent Cu-Al_2O_3 catalyst shows new additional peaks apart from the Cu metallic phase (Figure 7a) which have been ascribed to the formation of AlO(OH) boehmite structure (JCPDS 83-1506). This point is corroborated by the FT-IR spectrum (Figure SI5b) which also exhibits the characteristic vibrational modes of boehmite.[51] More evidence of the formation of nano-AlO(OH) are provided by TEM (Figure 7b), detecting wire-like fibres (length = 15 - 25 nm; width = 2 - 5 nm) related with random orientations of boehmite layers.

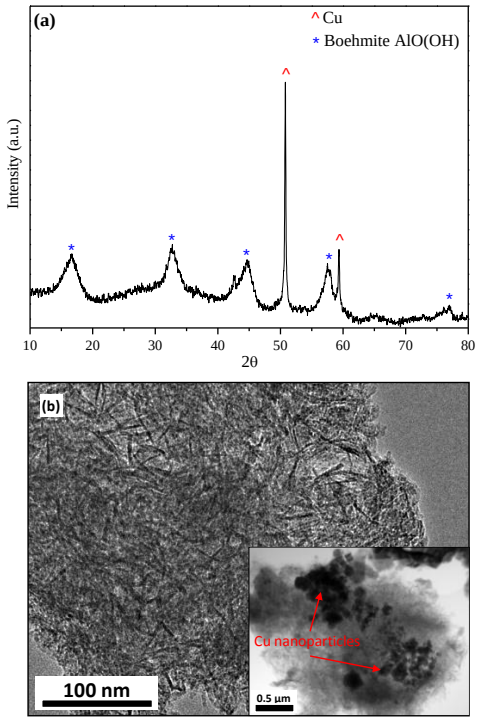

Figure 7. (a) XRD pattern and (b) TEM images of the used Cu-Al_2O_3 catalyst.

Thus, we can conclude that the Cu-Al_2O_3 catalyst is partially hydrated in the course of the reaction forming the AlO(OH) boehmite phase. These structural changes have been previously reported for impregnated metal alumina catalysts working under aqueous phase reforming conditions, leading to catalytic deactivation.[52,53]

In order to study the reusability of the spent Cu-Al_2O_3 catalyst, three consecutive reactions were conducted. Figure 8 represents HMF conversion and the yields of the main products after each run. The results show a gradual decrease of HMF conversion from 100 % to 76 % after three runs. Likewise, formation of HCPN decreases from 81 to 21 % after 3 cycles and the yield of the key intermediate FDM increases from 10 to 45 %. This progressive catalyst deactivation is associated with the observed hydration of the alumina phase towards boehmite which involves reduction of both acidity and specific surface area, along with an agglomeration of supported Cu particles.[52] In this respect, TEM images of the spent catalyst (Figure 7b inset) and EDX mapping (Figure SI6) show a significant decrease in the dispersion of the Cu nanoparticles over the alumina support compared to the fresh material (Figure SI2b). Regardless, a significant restoration of catalytic activity was observed (Figure 8; run 4) after a regeneration treatment of the used sample (air calcination 500 °C + H_2 reduction 500 °C). According to the X-ray diffraction of the regenerated catalyst (Figure SI7a), the recovery of the catalytic activity can be associated to the removal of boehmite phase, maintaining a Cu particle size (≈ 45 nm) comparable to the initial catalyst.

A similar characterization analysis was carried out on the used Co-Al_2O_3 catalyst (Figure 9). The obtained XRD pattern of the used Co-Al_2O_3 sample corresponds to an essentially amorphous material (Figure 9a). Compared to the X-ray diffraction pattern of the fresh material (Figure 3b), the diffraction peaks ascribed to the metallic cobalt phase disappear completely, whereas traces of Co_3O_4 are observed. The FT-IR spectrum (Figure SI8b) shows the characteristic bands of layered double hydroxide materials,[54] which can be attributed to the partial retention of the morphology of the precursor as a consequence of the reported "memory effect" of hydrotalcites.[55] Likewise, some minor bands related to the formation of hydrated boehmite were also observed at 1070 and 730 cm^{-1}. In accordance with the XRD pattern, TEM images of the used Co-Al_2O_3 catalyst reveal important differences with respect to the morphology of the fresh sample (Figure SI2c). Thus, the previously observed relatively large particles of metallic cobalt (≈28 nm) are not seen in the micrograph represented in Figure 9b. In contrast, well-dispersed nanoparticles (2 - 4 nm) with spherical shape can be observed (Figure 9b). Therefore, it seems that during the reaction, the metallic cobalt particles undergo oxidation and segregation, resulting in the formation of Co_3O_4 nanoparticles. This phenomenon could be related to the morphological changes observed in other Co-based catalysts, whose initial metallic particles are firstly transformed into hollow oxide spheres (based on Kirkendall effects), which finally break up into smaller particles under hydrogen atmospheres.[56] The oxidation rate of the Co-Al_2O_3 catalyst could be reduced by adding promoters, such as Pd,[57] or by selecting an appropriate H_2/H_2O partial pressure ratio and controlling cobalt crystallite sizes.[58]

The reusability of Co-Al_2O_3 catalyst was also checked by performing a consecutive run after recovering the spent catalyst. Figure 10 shows the activity of the reused sample after drying at 20 °C (Run 2a) and 120 °C (Run 2b). Thus, after the first run, a pronounced decrease in HMF conversion (14 - 16 %) was observed and HCPL was not formed at all. These results are in accordance with the catalytic activity showed by Zn-Al_2O_3 and Mg-Al_2O_3 catalysts in which the absence of a reduced metallic phase limited the formation of further hydrogenated products.

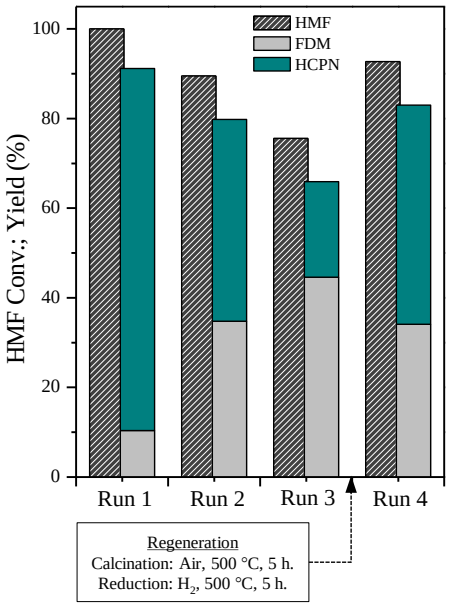

Figure 8. Conversion of HMF and yields of FDM and HCPL after 6 h reaction over the Cu-Al_2O_3 catalysts (T = 140 °C, P = 20 bar).

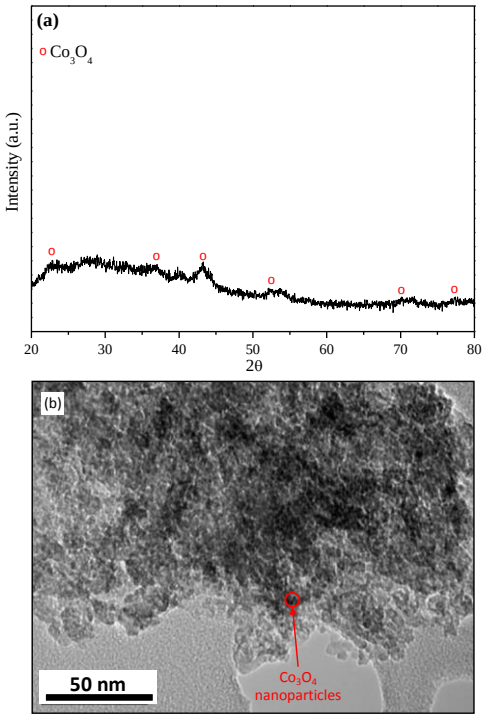

Figure 9. (a) XRD pattern and (b) TEM images of the used Co-Al_2O_3 catalyst.

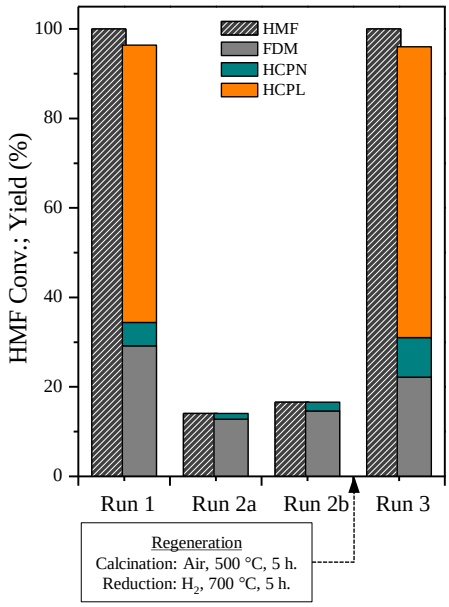

Figure 10. Conversion of HMF and yields of FDM, HCPN and HCPL after 6 h reaction over the Co-Al_2O_3 catalysts (T=140 °C, P=20 bar). Run 2a after drying at 20 °C and Run 2b after drying at 120 °C.

Hence, the oxidation of metallic Co into Co_3O_4 nanoparticles during the course of the reaction is most likely responsible for deactivation. To reverse the catalyst deactivation, a regeneration treatment (air calcination at 500 °C followed by H_2 reduction at 700 °C) was applied to the used Co-Al_2O_3 catalyst. The XRD pattern of the regenerated Co-Al_2O_3 sample (Figure SI7b) presents the peaks associated to the Co metallic phase, with a mean particle size around 20 nm. Thus, following these regeneration steps, the catalyst completely recovered its activity (Figure 10; Run 3), showing full conversion of HMF and a high selectivity to the targeted HCPL (65 %).

Conclusions

The highly selective production of HCPN (86 %) and HCPL (94 %) has been achieved over Cu-Al_2O_3 and Co-Al_2O_3, respectively, emphasizing an efficient catalytic route to produce cyclopentanone derivatives from HMF with readily available non-noble metals. The followed synthesis method resulted in well dispersed metal phases on alumina supports, exhibiting high specific surface areas and acid/base properties. At T > 160 °C and P_{H2} > 35 bar, the Cu-Al_2O_3 catalyst showed a complete conversion of HMF into the targeted HCPN and HCPL, whose yields can be tailored by varying the reaction conditions. On the other hand, the Co-Al_2O_3 catalyst showed a higher selectivity to the production of HCPL, a cyclic diol whose formation from biomass derived resources is reported for the first time.

The role of the metal and the acid/basic sites in the reaction mechanism has been elucidated based on the correlation between the main conversion pathways and the characterised catalytic properties (Figure 6). Reduced metal phases were crucial to promote the involved hydrogenation steps, whereas acid/basic sites were proved to be necessary for the extent of ring-opening/closure reactions. Thus, the combination of these functionalities on both Cu-Al_2O_3 and Co-Al_2O_3 favoured the formation of HCPN, which was rapidly hydrogenated to HCPL in presence of Co^0.

The reusability studies performed with the Cu-Al_2O_3 catalyst suggested a progressive deactivation related to the formation of hydrated boehmite phase (AlO(OH)). Likewise, the used Co-Al_2O_3 sample showed a poor activity after the first cycle due to the formation of Co_3O_4 nanoparticles. However, both structural changes were reversed by a simple regeneration treatment (air calcination at 500 °C followed by a H_2 reduction step), resulting in a significant restoration of their catalytic activities.

Acknowledgements

This work was supported by the Engineering and Physical Sciences Research Council (EPSRC), UK (EP/K014749). The MicroBioRefinery (MBR, University of Liverpool) is kindly acknowledged for providing the equipment for NH_3 and CO_2 chemisorption experiments.

References

1 R. Rinaldi and F. Schüth, *ChemSusChem*, 2009, **2**, 1096.
2 R. W. Torget, J. S. Kim and Y. Y. Lee, *Ind. Eng. Chem. Res*., 2000, **39**, 2817.
3 K. Yan, G. Wu, T. Lafleur and C. Jarvis, *Renew. Sust. Energ. Rev*., 2014, **38**, 663.
4 Y. Román-Leshkov, J. N. Chheda and J. A. Dumesic, *Science*, 2006, **312**, 1933.
5 R. J. van Putten, J. C. van der Waal, E. D. De Jong, C. B. Rasrendra, H. J. Heeres and J. G. de Vries, *Chem. Rev.*, 2013, **113**, 1499.
6 J. P. Lange, E. van der Heide, J. van Buijtenen and R. Price, *ChemSusChem*, 2012, **5**, 150.
7 Y. Nakagawa, M. Tamura and K. Tomishige, *ACS Catal.*, 2013, **3**, 2655.
8 A. Villa, M. Schiavoni, S. Campisi, G. M. Veith and L. Prati, *ChemSusChem*, 2013, **6**, 609; b) O. Casanova, S. Iborra and A. Corma, *ChemSusChem*, 2009, **2**, 1138.
9 R. Alamillo, M. Tucker, M. Chia, Y. Pagán-Torres and J. A. Dumesic, *Green Chem.*, 2012, **14**, 1413; b) Y. Nakagawa, K. Takada, M. Tamura and K. Tomishige, *ACS Catal*., 2014, **4**, 2718.
10 a) M. Chidambaram and A. T. Bell, *Green Chem*., 2010, **12**, 1253; b) Y. Román-Leshkov, C. J. Barrett, Z. Y. Liu and J. A. Dumesic, *Nature*, 2007, **447**, 982; c) D. P. Duarte, R. Martínez and L. J. Hoyos, *Ind. Eng. Chem. Res*., 2015, **55**, 54.
11 V. Choudhary, S. H. Mushrif, C. Ho, A. Anderko, V. Nikolakis, N. S. Marinkovic, A. I. Frenkel, S. I. Sandler and D. G. Vlachos, *J. Am. Chem. Soc.*, 2013, **135**, 3997; b) B. Girisuta, L. P. B. M. Janssen and H. J. Heeres, *Green Chem*., 2006, **8**, 701.
12 a) J. Tuteja, H. Choudhary, S. Nishimura and K. Ebitani, *ChemSusChem*, 2014, **7**, 96; b) T. Buntara, S. Noel, P. H. Phua, I. Melián-Cabrera, J. G. de Vries and H. J. Heeres, *Top. Catal.* 2012, **55**, 612; c) S. Yao, X. Wang, Y. Jiang, F. Wu, X. Chen and X. Mu, *ACS Sust. Chem. Eng*., 2013, **2**, 173.

13 J. Ohyama, R. Kanao, A. Esaki, A. Satsuma, *Chem. Commun*., 2014, **50**, 5633.
14 M. Hronec and K. Fulajtarová, *Catal. Commun*., 2012, 24, 100;
15 M. Renz, *Eu. J. Org. Chem*., 2005, **6**, 979.
16 K. A. Dubkov, G. I. Panov, E. V. Starokon, and V. N. Parmon, *React. Kinet. Catal. L*., 2002, **77**, 197.
17 T. Akashi, S. Sato, R. Takahashi, T. Sodesawa and K. Inui. *Catal. Commun*., 2003, **4**, 411.
18 J. N. Chheda, G. W. Huber and J. A. Dumesic, *Angew. Chem. Int. Ed*., 2007, **46**, 7164.
19 A. A. Rosatella, S. P. Simeonov, R. F. Frade, and C. A. Afonso, *Green Chem*., 2011, **13**, 754.
20 a) M. Hronec, K. Fulajtárová, I. Vávra, T. Soták, E. Dobročka and M. Mičušík, *Appl. Catal. B: Environ*., 2016, **181**, 210; b) Y. Yang, Z. Du, Y. Huang, F. Lu, F. Wang, J. Gao and J. Xu, *Green Chem.*, 2013, **15**, 1932; c) X. L. Li, J. Deng, J. Shi, T. Pan, C. G. Yu, H. J. Xu and Y. Fu, *Green Chem*., 2015, **17**, 1038; d) Y. Wang, M. Zhou, T. Wang and G. Xiao, *Catal. Lett.*, 2015, **145**, 1557; e) M. Zhou, H. Zhu, L. Niu, G. Xiao and R. Xiao, *Catal. Lett.*, 2014, **144**, 235.
21 J. Ohyama, R. Kanao, Y. Ohira, A. Satsuma, *Green Chem*., 2016, **18**, 676.
22 N. Perret, A. Grigoropoulos, M. Zanella, T. D. Manning, J. B. Claridge and M. J. Rosseinsky, *ChemSusChem*, 2016, **9**, 521.
23 V. Rives and M. A. Ulibarri, *Coord. Chem. Rev.*, 1999, **181**, 61.
24 L. Balduzzi, F. Prinetto, G. Ghiotti, A. Bianchini, M. Livi and A. Vaccari, *Stud. Surf. Sci. Catal.*, 2001, **140**, 67.
25 U. Constantino, F. Marmottini, M. Nocchetti and R. Vivani, Eur. *J. Inorg. Chem*., 1998, 1439.
26 F. Cavani, F. Trifirò and A. Vaccari, *Catal. Today*, 1991, **11**, 173.
27 J. J. Yu, Z. Jiang, L. Zhu, Z. P. Hao and Z. P. Xu, J. *Phys. Chem. B*, 2006, **110**, 4291.
28 A. Alejandre, F. Medina, P. Salagre, X. Correig and J. E. Sueiras, *Chem. Mater.*, 1999, **11**, 939.
29 Y. Lwin, M. A. Yarmo, Z. Yaakob, A. B. Mohamad and W. R. W. Daud, *Mater. Res. Bull.*, 2001, **36**, 193.
30 V. Muñoz, F. M. Z. Zotin and L. A. Palacio, *Catal. Today*, 2015, **250**, 173.
31 B. Jongsomjit, J. Panpranot and J. G. Goodwin, *J. Catal.*, 2001, **204**, 98.
32 F. Kovanda, T. Rojka, P. Bezdička, K. Jirátová, L. Obalová, K. Pacultová, Z. Bastl and T. Grygar, *J. Solid State Chem*., 2009, **182**, 27.
33 F. E. López-Suárez, A. Bueno-López and M. J. Illán-Gómez, *Appl. Catal. B: Environ.*, 2008, **84**, 651.
34 M. F. Luo, P. Fang, M. He and Y. L. Xie, J. *Mol. Catal. A: Chem.,* 2005, **239**, 243.
35 W. Chu, P. A. Chernavskii, L. Gengembre, G. A. Pankina, P. Fongarland and A. Y. Khodakov, *J. Catal.*, 2007, **252**, 215.
36 R. Bechara, D. Balloy, J. Y. Dauphin and J. Grimblot, *Chem. Mater.*, 1999, **11**, 1703.
37 a) A.Y. Khodakov, J. Lynch, D. Bazin, B Rebours, N Zanier, B. Moisson and P. Chaumette, *J. Catal.*, 1997, **168**, 16; b) G. Jacobs, Y. Ji, B.H. Davis, D. Cronauer, A.J. Kropf, and C.L. Marshall, *Appl. Catal. A: Gen.*, 2007, **333**, 177.
38 H. A. Oliveira, D. F. Franceschini and F. B. Passos, *J. Braz. Chem. Soc*., 2014, **25**, 2339.
39 K. Lourvanij, PhD thesis, Partial dehydration of glucose to oxygenated hydrocarbons in molecular-sieving catalysts, Oregon State University, 1995.
40 C. O. Veloso, C. N. Pérez, B. M. de Souza, E. C. Lima, A. G. Dias, J. L. F. Monteiro and C. A. Henriques, *Microp. Mesop. Mater.*, 2008, **107**, 23.
41 J. I. Di Cosimo, V. K. Diez, M. Xu, E. Iglesia and C. R. Apesteguia, *J. Catal.*, 1998, **178**, 499.
42 S. F. Wang, G. Z. Sun, L. M. Fang, L. Lei, X. Xiang and X. T. Zu, *Scientific Reports*, 2015, 5.
43 Y. Nakagawa and K. Tomishige, *Catal. Commun*., 2010, **12**, 154.
44 S. Sitthisa and D. E. Resasco, *Catal. Lett*., 2011, **141**, 784.
45 P. Gallezot, A. Giroir-Fendler and D. Richard, *Catal. Lett*., 1990, **5**, 169.
46 P. Claus, *Top. Catal*., 1998, **5**, 51.
47 F. Liu, M. Audemar, K. D. O. Vigier, J. M. Clacens, F. De Campo and F. Jérôme, *ChemSusChem*, 2014, **7**, 2089.
48 F. Liu, M. Audemar, K. D. O. Vigier, J. M. Clacens, F. De Campo and F. Jérôme, *Green Chem*., 2014, **16**, 4110.
49 V. I. Baranenko and V. S. Kirov, *At. Energ*., 1989, **66**, 30.
50 S. Sitthisa, T. Sooknoi, Y. Ma, P. B. Balbuena and D. E. Resasco, *J. Catal*., 2011, **277**, 1.
51 S. G. Wang, Y. Ma, Y. J. Shi and W. X. Gong, *J. Chem. Tech. Biotech*., 2009, **84**, 1043.
52 R. M. Ravenelle, J. R. Copeland, W. G. Kim, J. C. Crittenden and C. Sievers, *ACS Catal*., 2011, **1**, 552.
53 H. Li, Y. Zhao, C. Gao, Y. Wang, Z. Sun and X. Liang, *Chem. Eng. J*., 2012, **181**, 501.
54 J. T. Kloprogge and R. L. Frost, *J. Solid State Chem*., 1999, **146**, 506.
55 Q. Liu, B. Wang, C. Wang, Z. Tian, W. Qu, H. Ma and R. Xu, *Green Chem*., 2014, **16**, 2604.
56 A. M. Saib, D. J. Moodley, I. M. Ciobîcă, M. M. Hauman, B. H. Sigwebela, C. J. Weststrate, J. W. Niemantsverdriet and J. Van de Loosdrecht, *Catal. Today*, 2010, **154**, 271.
57 T. Nowitzki, A. F. Carlsson, O. Martyanov, M. Naschitzki, V. Zielasek, T. Risse, M. Schmal, H-J. Freund and M. Bäumer, *J. Phys. Chem. C*, 2007, **111**, 8566.
58 E. van Steen, M. Claeys, M.E. Dry, J. van de Loosdrecht, E.L. Viljoen and J.L. Visagie. *J. Phys. Chem. B*, 2005, **109**, 3575.